Published in final edited form as:
Channels (Austin). 2008 ; 2(4): 278–282.

A mutually exclusive alternative exon of *slo1* codes for a neuronal BK channel with altered function

Malle Soom[1,#], **Guido Gessner**[1,#], **Heike Heuer**[2], **Toshinori Hoshi**[3], and **Stefan H. Heinemann**[1,*]

[1] Center for Molecular Biomedicine, Department of Biophysics, Friedrich Schiller University Jena, Hans-Knöll-Str. 2, D-07745 Jena, Germany

[2] Fritz Lipmann Institute for Age Research, Research Unit Neuroendocrinology, Beutenbergstr. 11, D-07745 Jena, Germany

[3] Department of Physiology, University of Pennsylvania, 3700 Hamilton Walk, Philadelphia, PA 19104, USA

Abstract

Large-conductance Ca^{2+}- and voltage-activated K^+ (BK) channels are comprised of four pore-forming α-subunits (Slo1), whose mRNA is alternatively spliced in a cell-specific manner. Here we report the first case of a correctly spliced mutually exclusive exon in a mammalian BK channel; an exon coding for the region from S6 to the RCK1 domain is exchanged for an alternative exon of the same length. The Slo1 transcript with this novel exon is present in native brain tissues and inclusion of the alternative exon profoundly alters the channel's gating characteristics: faster activation at low Ca^{2+} concentrations and greater open probability at resting membrane potential at high Ca^{2+} concentrations. The novel gating features conferred by the alternative exon are dominant over those of the commonly described Slo1 variant when coexpressed. These data show that evolutionary preserved regulation of alternative Slo1 splicing of the S6-RCK1 linker creates fine-tuning of neuronal excitability.

Keywords

Slo1; BK channels; gene splicing; Ca^{2+} dependence; K(Ca^{2+}); KCNMA1

INTRODUCTION

Large-conductance Ca^{2+}- and voltage-activated K^+ channels (BK, also termed BK_{Ca}, Slo1, MaxiK or $K_{Ca}1.1$) open in response to depolarization or an increase in intracellular Ca^{2+} concentration ($[Ca^{2+}]_i$) to mediate K^+ efflux. Voltage sensing of the channel involves select residues in the transmembrane segments (S0–S6) and the Ca^{2+} sensors are located in/near the two cytoplasmic domains termed RCK1 and RCK2 (Magleby 2003). Both sensors allosterically control the ion conduction gate located in the transmembrane segment S6 (Jiang *et al*, 2002). The allosteric nature of the gating allows BK channels to participate in a broad range of functions: action potential repolarization, neuronal excitability, neurotransmitter release, hormone secretion, tuning of cochlear hair cells, modulation of the

[*]Address correspondence to SHH: phone: ++49-3641-9 39 56 50, fax: ++49-3641-9 39 56 52, stefan.h.heinemann@uni-jena.de.
[#]Authors contributed equally

CONFLICT OF INTEREST
The authors declare that they have no conflict of interest.

tone of smooth muscles, and tumor proliferation (Ghatta *et al*, 2006; Salkoff *et al*, 2006). The remarkable physiological versatility of BK channels results from post-translational modifications, coassembly with other interacting proteins, and splicing of the channel transcript.

Only one human gene (*slo*1 or KCNMA1) coding for the pore-forming α-subunit of BK channels exists but the transcript is extensively alternatively spliced. To date, at least nine alternative splicing sites and over 20 individual splice variants have been reported for vertebrate *slo*1 (Fettiplace & Fuchs, 1999; Lu *et al*, 2006; Beisel *et al*, 2007) (Fig 1A). While most variants result from insertions of cassette exons (e.g. Zarei *et al*, 2001), some variants represent exon deletions (e.g. Chen *et al*, 2005) and intron retention (e.g. Bell *et al*, 2008). However, no usage of mutually exclusive alternative exons to product functional BK channels has been demonstrated for mammalian *slo*1 (Copley 2004). In *Drosophila slo*1 (Lagrutta *et al*, 1994) one of three mutually exclusive alternative exons can be spliced into a region corresponding to the C-terminal end of S6 and the beginning of the cytoplasmic RCK1 domain of the protein. An alternative exon for this S6-RCK1 linker segment may exist in mice as suggested by one EST clone (BY742482); however, inclusion of this exon results in a frameshift and would consequently lead to expression of truncated non-functional channels.

Here we report the existence of a correctly spliced human *slo*1 transcript utilizing a mutually exclusive alternative exon targeting the S6-RCK1 linker segment, a crucial area for the channel's gating, and show that alternative splicing of this exon occurs mainly in brain tissues and results in functional channels with strongly altered gating characteristics.

RESULTS AND DISCUSSION

Cloning of novel slo1 splice variants from human LNCaP cells

Searching for the molecular correlate of the BK_L channel found in human LNCaP prostate cancer cells to activate appreciably at negative voltages in the absence of Ca^{2+} (Gessner *et al*, 2006), we isolated a number of cDNA fragments enoding Slo1 from such cells. From 38 cloned PCR fragments covering the region from S3 to RCK1 we found one novel human *slo*1 splice variant of particular interest generated by exchange of exon 9 (e9, see Methods) with an alternative exon of the same length (e9alt) starting 104 bp downstream of e9 (Fig 1A). In addition, we identified four further alternative *slo*1 splicing events as summarized in suppl. Fig 1. All these splice variants, except for e9alt, produce a frameshift and should result in premature termination of Slo1 protein synthesis in the region between S6 and S9 and thus are expected to lack functional expression (Chen *et al*, 2005; Davies *et al*, 2007). Therefore, we concentrated on the splicing event characterized by e9alt. Exon 9 is 92 bp long and encodes 31 aa comprising the end of the S6 domain, the S6-RCK1 linker and the beginning of the RCK1 domain (Fig 1C and suppl. Fig 2). E9 and e9alt share 61.3% homology on the nucleotide level and 58% homology on the amino acid level. Analysis of genomic sequences showed that e9, e9alt, and their flanking intronic sequences are highly conserved in vertebrates, suggesting that splicing of the alternative exon 9 is a wide-spread phenomenon in a variety of vertebrate species.

Expression of a novel slo1 variant

Expression analysis by RT-PCR showed the presence of e9alt-containing transcripts in select human cell lines including LNCaP, the mammacarcinoma cell line T47D, and a primary glioma cell line (G290). The cell-line specific expression of e9alt is suggested by the lack of RT-PCR signal in neuroblastoma and smooth muscle cells (Fig 2Aa).

To verify usage of e9alt in native tissues we performed e9/e9alt specific RT-PCRs with RNA isolated from various mouse tissues. For both variants, PCR products were of the expected size (Fig 2Ab). Products obtained from cerebellum were sequenced and revealed the expected DNA sequence. In 90-days old mice, the signal corresponding to e9alt was obtained exclusively from brain samples. Quantitative real-time PCR showed that the ratio of *slo*1 e9alt to e9 in LNCaP cells and mouse cerebellum was 1:117 and 1:24, respectively (Fig 2B). Brain samples of 21-days old mice also showed e9alt signals (Fig 2Ac) while expression of e9alt was not detected in day-18 embryonal tissues (not shown), indicating a developmental regulation of e9 splicing.

We verified the brain expression pattern of e9alt transcripts by *in situ* hybridization analysis. Whereas the corresponding sense probes did not produce any specific labeling above background, hybridization of the e9-specific riboprobe revealed an mRNA distribution pattern with highest transcript levels throughout the cerebral cortex, in pyramidal and granule cells of the hippocampus, in cerebellar Purkinje cells, and in the olfactory bulb (Fig 2C), which is a similar pattern as that observed by Sausbier *et al* (2004). The hybridization signals obtained with the e9alt-specific probe showed the same distribution pattern but were weaker and required an exposure time of three days compared to the signals of e9 (one day exposure) (Fig 2C). Competition experiments performed by adding unlabelled probe to the labeled showed that the e9alt probe was not able to compete with the e9 probe and vice versa.

How is mutually exclusive e9/e9alt splicing regulated? A weaker splicing 5′ acceptor site in e9alt compared with e9, as predicted by NetGene2 (www.cbs.dtu.dk/services/NetGene2), may explain the low abundance of e9alt containing transcripts. Future experiment, however, are necessary to clarify why e9alt usage is restricted to brain tissue and certain cancer cells.

Electrophysiological properties of the novel Slo1 e9alt variant

Electrophysiological assays revealed clear functional differences between the Slo1 e9 and e9alt channels expressed in HEK 293 cells. In the virtual absence of intracellular Ca^{2+}, Slo1 e9alt channels (Fig 3A, B, *middle*) activated with much smaller depolarization (≥50 mV) than Slo1 e9 channels (≥100 mV) (Fig 3A, B, *left*). Voltage and Ca^{2+} dependence of channel activation was assayed by measuring peak tail currents following 10-ms pulses to varying voltages in varying $[Ca^{2+}]_i$. Such data, shown for 0 and 100 μM Ca^{2+} in Fig 3B, revealed that Slo1 e9alt channels exhibit a much shallower activation curve and a reduced impact of Ca^{2+} on the half-maximal activation voltage. Moreover, Slo1 e9alt channels were open at resting voltages in high $[Ca^{2+}]$ (Fig 3B, *middle*; for detailed analysis of the voltage dependence see suppl. Fig 4). The greater baseline channel activity of Slo1 e9alt is also manifested in the small but significant inward currents at −150 mV (Fig 3A, *arrows*).

Activation kinetics of Slo1 e9alt was markedly faster than that of Slo1 e9 in 0 Ca^{2+}. Increasing $[Ca^{2+}]$ accelerated activation of both variants and at $[Ca^{2+}]$ =100 μM, the difference became indistinguishable (Fig 3C). Marked difference in deactivation was also observed between the two variants but the Ca^{2+} dependence was opposite in that deactivation time courses at −150 mV were indistinguishable in 0 Ca^{2+}, while in 100 μM Ca^{2+} Slo1 e9alt deactivated about 3-fold faster than Slo1 e9 (Fig 3D).

Recordings from cells expressing both variants showed marked channel activation at low voltages (Fig 3A,B, *right*), resembling the Slo1 e9alt behavior. Voltage dependence of activation was intermediate to data of homomeric channels (suppl. Fig 4). Activation kinetics was similar to that of Slo1 e9, whereas deactivation was indistinguishable from Slo1 e9alt (Fig 3C,D). Thus, e9alt alters channel gating and both Slo1 variant subunits are able to form heteromeric channels.

Assaying the ion selectivity of Slo1 e9alt channels under biionic conditions revealed an about 30-fold higher permeability for K^+ over Na^+ and Li^+ indicating that K^+ selectivity is preserved. In addition, both variants were completely blocked by 2 mM extracellular tetraethylammonium (not shown).

Slo1 e9 and e9alt channels were further compared on the single-channel level. All-points histograms for Slo1 e9 channels at +50 mV allowed distinguishing between closed and open-channel current levels (Fig 4A). By contrast, Slo1 e9alt channel openings were much less stable compromising the detection of discrete current levels (Fig 4B). At negative voltages, both channel types exhibited short opening events that were subjected to single-channel analysis (Fig 4C), excluding events shorter than 40 μs. In symmetrical (140 mM) K^+, the single-channel conductance of Slo1 e9 channels of 204 ± 5 pS (*n*=4) significantly (*P*=0.007) exceeded the 135 ± 9 pS (*n*=3) of Slo1 e9alt channels. Mean open lifetime, derived from single-exponential fits to lifetime histograms (Fig 4C), was about twice as long (*P*=0.008) for Slo1 e9 compared with Slo1 e9alt channels (e9: 134 ± 15 μs, *n*=8; e9alt: 58 ± 9 μs, *n*=6). In accordance to macroscopic data, activity of Slo1 e9alt channels at low voltages could be strongly enhanced by increasing $[Ca^{2+}]_i$ (data not shown). Open probability of Slo1 e9alt channels at −50 mV (>0.01%, 3 patches) was substantially higher than for Slo1 e9 channels (<0.0015%, 4 patches). Note that data shown in Figs 4A and 4B are derived from patches containing more Slo1 e9 (~200) than e9alt channels (~10).

In summary we conclude that the sequence of the S6/RCK linker affects BK gating in a qualitatively different manner than the linker length (Niu *et al*, 2004). Whereas the latter produces shifts in *the* half-maximal activation voltage only, changes observed for Slo1 e9alt additionally concern the steepness of the voltage dependence, the ability of the channel to close at negative voltages, and the single-channel characteristics.

The reduced single-channel conductance and the flickery gating most likely result from aa changes I323A+E324A in Slo1 e9alt channels. A *Drosophila* A3 splice variant (corr. I323+D324) behaves similarly (Lagrutta *et al*, 1994). Guo *et al* (2008) proposed that reduced hydrophobicity at position 323, serving as hydrophobic gate, induces flickery gating and promotes sub-conductance states. However, those channels did not activate at resting voltages like the Slo1 e9alt variant. We, thus, conclude that the flickery gating and the lower single-channel conductance of Slo1 e9alt channels result from changes within the gate, whereas the inability to close at low potentials, in particular in high $[Ca^{2+}]$, must result from changes in the linker and/or the start of the RCK1 domain. The functional effects of specific amino acid exchanges suggest that the S6/RCK linker possess defined sable structures. However, in the crystal structure of MthK (Jiang *et al*, 2002), the corresponding region was disordered in the crystal structure of MthK (Jiang *et al*, 2002). Thus, we speculate that linker segment switches between different conformations during channel gating. A loss of hydrophobic contacts necessary to keep the channel closed at negative potentials in part mediated by the amino acid at position 323 may account for the high voltage-independent activity of Slo1 e9alt channels.

Since Slo1 e9 and e9alt proteins can form heteromeric channels, we suggest that a small population of BK channels exhibits enhanced activity at low $[Ca^{2+}]$ and with smaller depolarizations, in fact even at resting membrane potential, especially at elevated $[Ca^{2+}]$. These features could enhance the established role of BK channels in promoting proliferation in various cancer cells (Coiret *et al*, 2006; Han *et al*, 2007; Weaver *et al*, 2004). Moreover, the unusual gating properties features may enable BK-expressing cells, such as cerebellar or hippocampal neurons to maintain the high-frequency (Sausbier *et al*, 2004; Gu *et al*, 2007). Thus, mutually exclusive *slo*1 e9/e9alt splicing may serve as a fine-tuning mechanism of neuronal firing.

METHODS

Cell culture and molecular biology

HEK 293 cells (DSMZ), LNCaP cells (DSMZ) and T74D cells (ATCC) were cultivated as described previously (Gessner *et al*, 2006) *hKCNMA1* (hSlo1, U11058) was subcloned into pCI-neo (Promega, Mannheim, Germany). PCR clones were ligated into pGEM-T vector (Promega). *Slo*1 e9alt expression clone was obtained by PCR using 2 clones with overlapping e9alt sequences. Resulting fragment comprising nt 550–1750 of *slo*1 was cloned into pCIneo *KCNMA1* vector using *Pac*I / *Pml*I restriction sites. All constructs were verified by sequencing. Human and mouse KCNMA1 exon nomenclature was according to: human (*Homo sapiens*) ENST00000358063; mouse (*Mus musculus*) ENSBTAT00000017701 (www.ensembl.org).

Human smooth muscle cells were prepared from Vena saphena, kindly provided by Dr. E. Bretschneider, FSU Jena. cDNAs from neuroblastoma cell line SH-SY5Y and human primary glioma cell line G290 were kindly provided by Dr. K. Schönherr and Dr. L. Pusch, FSU Jena. Sv129 mice tissues were kindly provided by C. König, FSU Jena. Total RNA extraction from cultured cells or tissues was performed with Qiagen RNA Easy Kit. First-strand cDNA was synthesized with SuperScript II or III cDNA synthesis Kit (Invitrogen). cDNAs were subjected to PCR analysis with Expand High Fidelity PCR Kit (Roche) (see suppl. Tables 1 and 2 for primer sequences and pairs here and below). Quantitative RT-PCR was performed on Mastercycler® *ep realplex* (Eppendorf) using Light Cycler RT-PCR Kit (Roche). Cycler conditions were as follows: 10 min initial denaturation; 36 cycles of 10 sec denaturation at 95ºC, 10 sec annealing at 59ºC, 20 sec extension at 72ºC. Specificity of oligos for detection of e9 and e9alt was validated prior to RT-PCR and quantitative RT-PCR experiments (suppl. Fig 3 and suppl. Tab 3).

In situ hybridization

Radiolabeled riboprobes were generated by *in vitro* transcription using e9- and e9alt-specific cDNA fragments from mouse cerebellum cloned in pGEMT vector as templates. ISH histochemistry was carried out on frozen sagittal mouse brain sections as previously described (Heuer *et al*, 2000; suppl. Methods). After hybridization, the sections were exposed to X-ray film (BioMax MR, Kodak) for one or three days.

Electrophysiology

Electrophysiological recordings were performed as described previously (Gessner *et al*, 2006). The external solution contained (in mM) 140 KCl, 2 $CaCl_2$, 2 $MgCl_2$, 10 HEPES, pH 7.4. For biionic measurements, NaCl or LiCl replaced KCl. The internal solution contained (in mM) 140 KCl, 10 HEPES, pH 7.4. Free [Ca^{2+}] were adjusted by addition of (in mM): 10 EGTA (nominally calcium free; calculated ca. 5 nM); 10 EGTA + 5.9 $CaCl_2$ (100 nM); 10 HEDTA + 3.3 $CaCl_2$ (1 μM); 10 HEDTA + 8.3 $CaCl_2$ (10 μM); 10 HEDTA + 9.9 $CaCl_2$ (100 μM). For analysis of the voltage dependence of channel activation see suppl. Fig 4. For single-channel analysis we used the 50% threshold method. The number of channels per patch was estimated based on the open probability as determined from macroscopic data, the single-channel conductance, and the current amplitude at +250 mV. Data are given as mean ± S.E.M. (*n*), with *n* = number of independent experiments. Statistical significant differences between groups of data were tested using two-sided Students t-test and ANOVA with Bonferroni's correction for multiple comparisons.

Supplementary Material

Refer to Web version on PubMed Central for supplementary material.

Acknowledgments

This study was supported by TMWFK/IZKF (B 307-04004, TP4.5) and DFG (SFB 604, TP A4).

References

Beisel KW, Rocha-Sanchez SM, Ziegenbein SJ, Morris KA, Kai C, Kawai J, Carninci P, Hayashizaki Y, Davis RL. Diversity of Ca^{2+}-activated K^+ channel transcripts in inner ear hair cells. Gene 2007;386:11–23. [PubMed: 17097837]

Bell TJ, et al. Cytoplasmic BK(Ca) channel intron-containing mRNAs contribute to the intrinsic excitability of hippocampal neurons. Proc Natl Acad Sci USA 2008;105:1901–1906. [PubMed: 18250327]

Chen L, Tian L, MacDonald SH, McClafferty H, Hammond MS, Huibant JM, Ruth P, Knaus HG, Shipston MJ. Functionally diverse complement of large conductance calcium- and voltage-activated potassium channel (BK) alpha-subunits generated from a single site of splicing. J Biol Chem 2005;280:33599–33609. [PubMed: 16081418]

Coiret G, Borowiec A-S, Mariot P, Ouadid-Ahidouch H, Matifat F. The antiestrogen tamoxifen activates BK channels and stimulates proliferation of MCF-7 breast cancer cells. Mol Pharmacol 2007;71:843–851. [PubMed: 17164406]

Copley RR. Evolutionary convergence of alternative splicing in ion channels. Trends Genet 2004;20:171–176. [PubMed: 15101391]

Davies KP, Zhao W, Tar M, Figueroa JC, Desai P, Verselis VK, Kronengold J, Wang HZ, Melman A, Christ GJ. Diabetes-induced changes in the alternative splicing of the slo gene in corporal tissue. Eur Urol 2007;52:1229–1237. [PubMed: 17150299]

Fettiplace R, Fuchs PA. Mechanisms of hair cell tuning. Annu Rev Physiol 1999;61:809–834. [PubMed: 10099711]

Gessner G, Schönherr K, Soom M, Hansel A, Asim M, Baniahmad A, Derst C, Hoshi T, Heinemann SH. BK_{Ca} channels activating at resting potential without calcium in LNCaP prostate cancer cells. J Membrane Biol 2006;208:229–240. [PubMed: 16604468]

Ghatta S, Nimmagadda D, Xu X, O'Rourke ST. Large-conductance, calcium-activated potassium channels: Structural and functional implications. Pharmacol Ther 2006;110:103–116. [PubMed: 16356551]

Gu N, Vervaeke K, Storm JF. BK potassium channels facilitate high-frequency firing and cause early spike frequency adaptation in rat CA1 hippocampal pyramidal cells. J Physiol 2007;580:859–882. [PubMed: 17303637]

Guo Z, Lv C, Yi H, Xiong Y, Wu Y, Li W, Xu T, Ding J. A residue at the cytoplasmic entrance of BK-type channels regulating single-channel opening by its hydrophobicity. Biophys J 2008;94:3714–3725. [PubMed: 18400952]

Han X, et al. Heat shock proteins and p53 play a critical role in K^+ channel-mediated tumor cell proliferation and apoptosis. Apoptosis 2007;12:1837–1846. [PubMed: 17624594]

Heuer H, Schäfer MK, O'Donnell D, Walker P, Bauer K. Expression of thyrotropin-releasing hormone receptor 2 (TRH-R2) in the central nervous system of rats. J Comp Neurol 2000;428:319–336. [PubMed: 11064370]

Jiang Y, Lee A, Chen J, Cadene M, Chait BT, MacKinnon R. Crystal structure and mechanism of a calcium-gated potassium channel. Nature 2002;417:515–522. [PubMed: 12037559]

Lagrutta A, Shen K-Z, North A, Adelman JP. Functional differences among alternatively spliced variants of *slowpoke*, a *Drosophila* calcium-activated potassium channel. J Biol Chem 1994;269:20347–20351. [PubMed: 8051129]

Lu R, Alioua A, Kumar Y, Eghbali M, Stefani E, Toro L. MaxiK channel partners: physiological impact. J Physiol 2006;570:65–72. [PubMed: 16239267]

Magleby KL. Gating mechanism of BK (Slo1) Channels: So near, yet so far. J Gen Physiol 2003;121:81–96. [PubMed: 12566537]

Niu X, Qian X, Magleby KL. Linker-gating ring complex as passive spring and Ca^{2+}-dependent machine for a voltage- and Ca^{2+}-activated potassium channel. Neuron 2004;42:745–756. [PubMed: 15182715]

Salkoff L, Butler A, Ferreira G, Santi C, Wei A. High-conductance potassium channels of the SLO family. Nat Rev Neurosci 2006;5:921–931. [PubMed: 17115074]

Sausbier M, et al. Cerebellar ataxia and Purkinje cell dysfunction caused by Ca^{2+}-activted K^{+} channel deficiency. Proc Natl Acad Sci USA 2004;101:9474–9478. [PubMed: 15194823]

Weaver AK, Liu X, Sontheimer H. Role for calcium-activated potassium channels (BK) in growth control of human malignant glioma cells. J Neurosci Res 2004;78:224–234. [PubMed: 15378515]

Zarei MM, Zhu N, Alioua A, Eghbali M, Stefani E, Toro L. A novel MaxiK splice variant exhibits dominant-negative properties for surface expression. J Biol Chem 2001;276:16232–16239. [PubMed: 11278440]

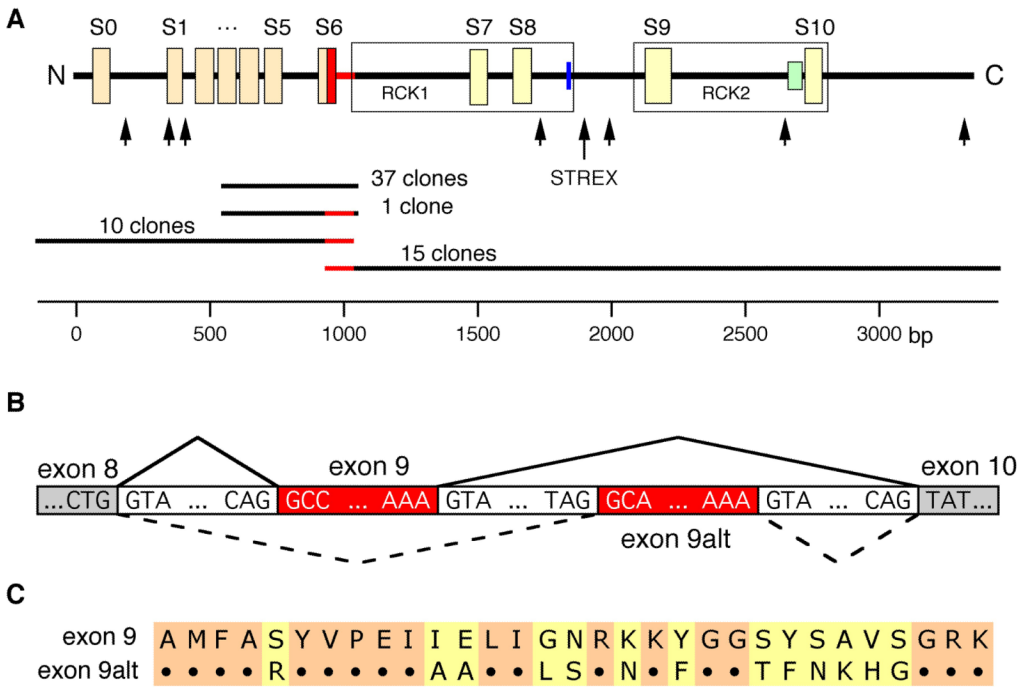

Fig 1.

Identification of splice products of *slo1* in human LNCaP cells. **(A)** upper panel: schematic view of hSlo1 structural elements: S0–S10 – hydrophobic domains; RCK1 and RCK2 regions (boxed); heme-binding site (blue); Ca^{2+}-bowl (green). Arrows designate sites of alternative splicing identified in mammalian *slo*1 mRNAs. Region corresponding to exon 9 is highlighted in red. Lower panel: clones used to identify transcripts with e9alt (red). Nucleotide positions according to *hslo*1 mRNA sequence U11058 are shown on the scale. **(B)** Schematic overview of the novel alternatively spliced exon 9 in *hslo*1 form LNCaP cells. **(C)** Alignment of the deduced amino acid sequences of *slo*1 exon 9 and exon 9alt (for nucleotide sequence see suppl. Fig 2).

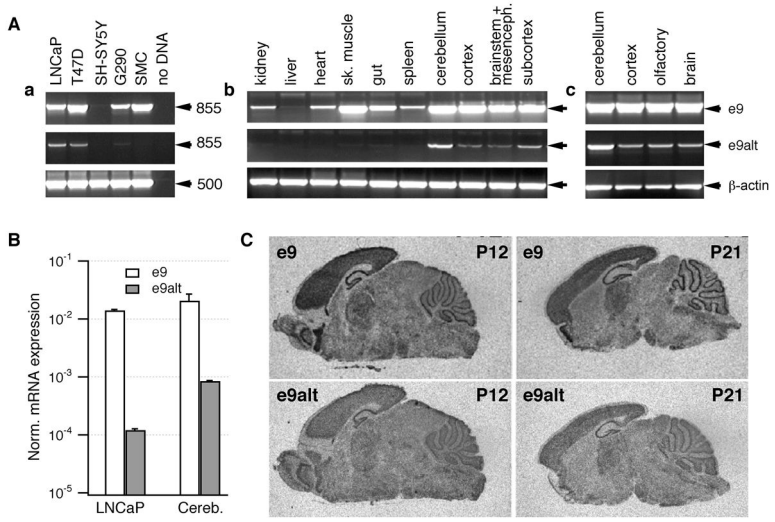

Fig 2.

Expression of *slo*1 e9 and e9alt splice variants in cell lines and native tissues. **(A)** *Slo*1 transcripts containing e9alt are predominantly expressed in native brain tissues. Representative results of RT-PCRs performed on mRNA isolated from human cell lines **(a)** and tissues from postnatal day 90 **(b)** and 21 **(c)** mice. T74D – human mammacarcinoma cell line; G290 – glioma primary cell line; SMC – vascular smooth muscle primary cell line. **(B)** Quantification of expression of *slo*1 transcripts containing e9 and e9alt in LNCaP cells and mouse cerebellum. Real-time RT-PCR data are normalized to β-actin expression levels and represented as average ± SD of 3 (LNCaP) or 2 (mouse cerebellum) parallel experiments. **(C)** E9 and e9alt transcripts exhibit similar distribution patterns in mouse brain. *In situ* hybridization of mouse brain slices from postnatal days 12 (P12, left) and 21 (P21, right) with probes against e9 (upper panels) and e9alt (lower panels). Films were exposed for 1 day (e9) or 3 days (e9alt).

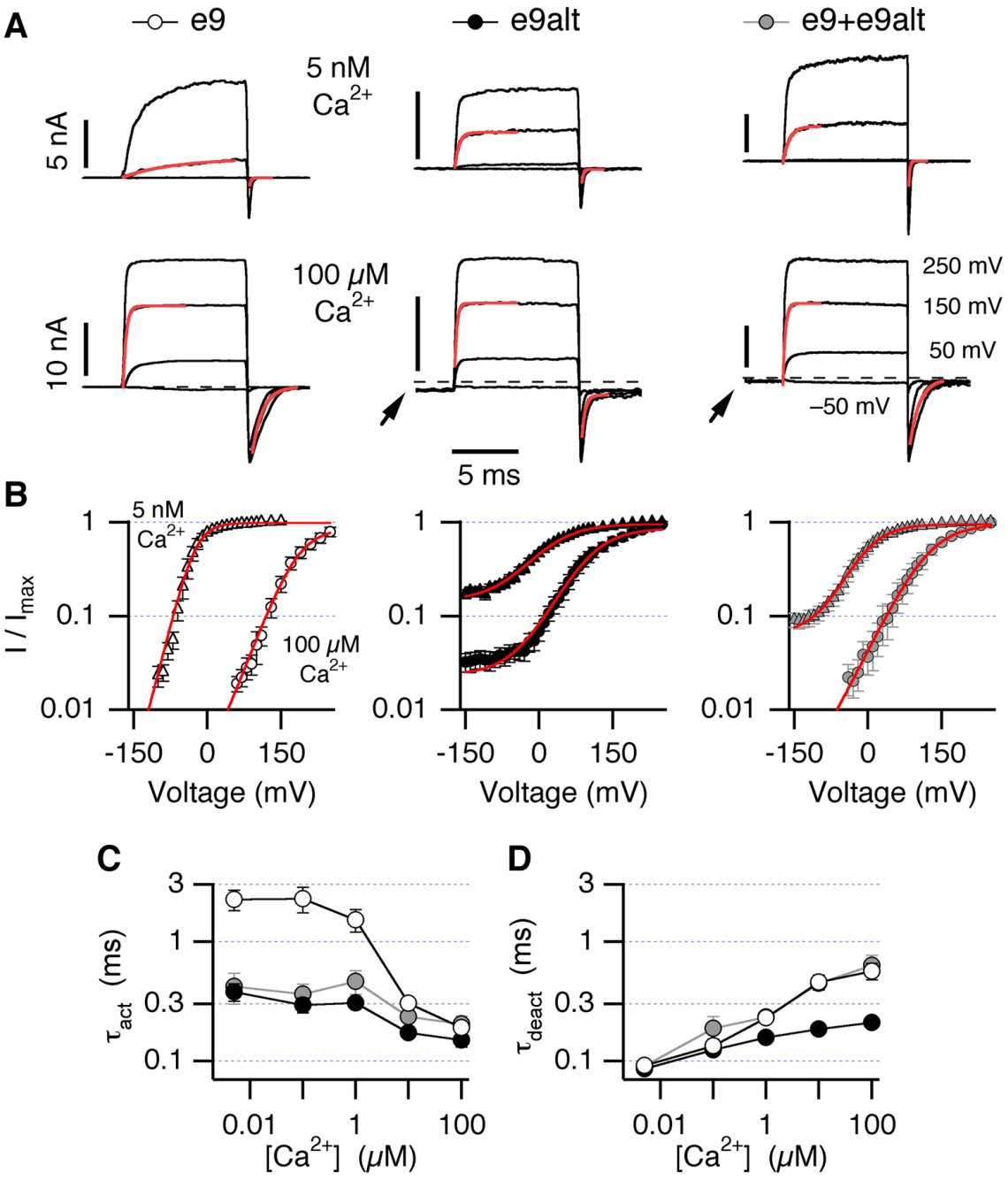

Fig 3.

Voltage- and Ca^{2+}-dependence of hSlo1 e9 and e9alt channels. **(A)** Macroscopic inside-out patch recordings from hSlo1 e9 and/or e9alt expressing HEK 293 cells in 0 (*top*) and 100 μM Ca^{2+} (*bottom*). Currents were elicited by 10-ms depolarizations to −50, 50, 150 and 250 mV from −150 mV. The dashed lines indicate zero current level. Arrows highlight the steady-state channel activity at −150 mV. **(B)** Normalized conductance-voltage plots obtained from the analysis of tail currents (as in **A)** with superimposed Boltzmann fits (see suppl. Fig 4). Time courses of activation at +150 mV and deactivation at −150 mV were fitted with mono-exponential functions (superimposed in **A**), yielding time constants plotted against $[Ca^{2+}]_i$ in **C** and **D**, respectively.

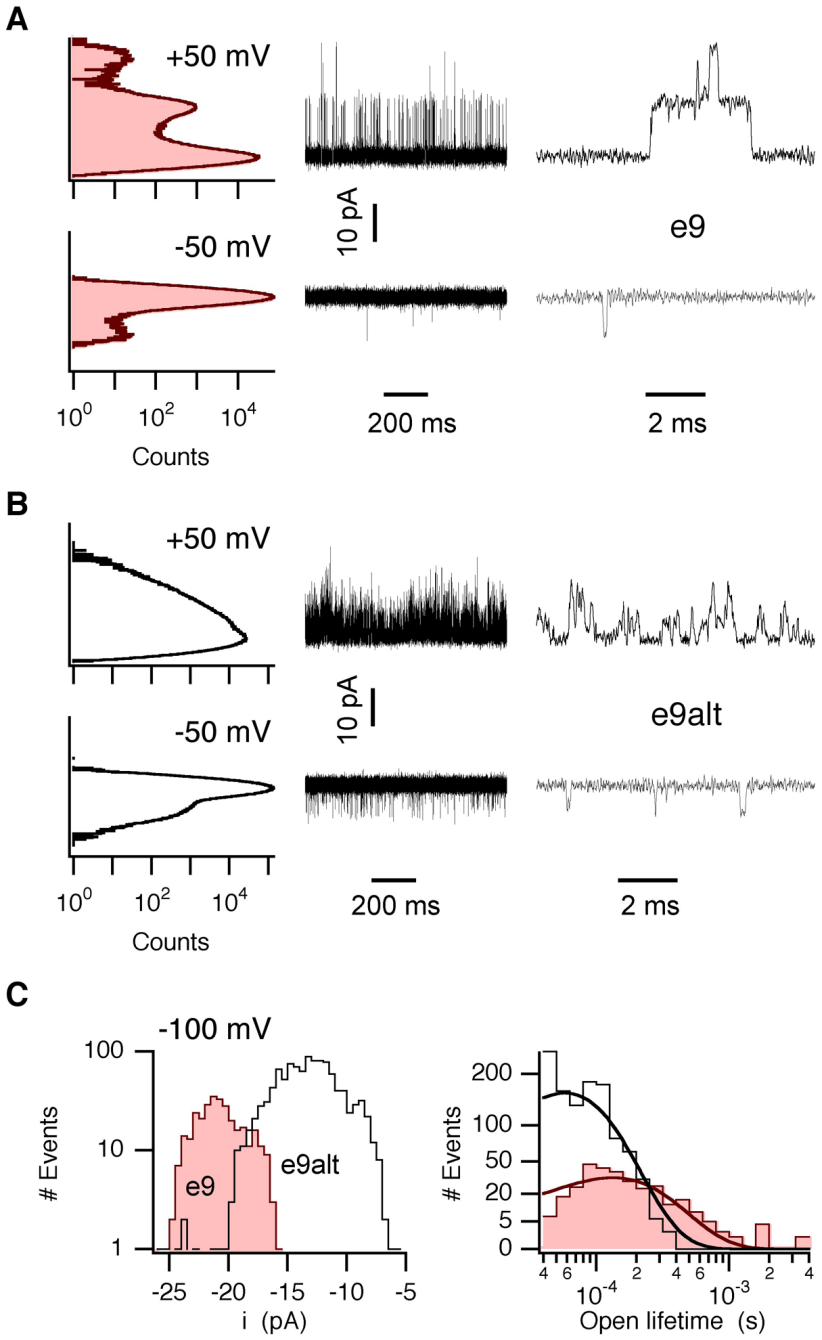

Fig 4.

Single-channel properties of hSlo1 e9 and e9alt channels. Inside-out patch recordings from Slo1 e9 **(A)** or e9alt **(B)** channels. Corresponding all-points amplitude histograms are shown left to the current traces. Representative events are shown on the right at higher time resolution. **(C)** Single-channel amplitude histograms (*left*) and open lifetime histograms (*right*) for Slo1 e9 and e9alt channels −100 mV. Superimposed curves represent exponential fits according to a probability-density function.